11th ANKARA INTERNATIONAL AEROSPACE CONFERENCE **AIAC-2021-089**
8-10 September 2021 - METU, Ankara TURKEY

AERODYNAMIC ANAYLSES OF THICK WIND TURBINE AIRFOIL FOR HIGH REYNOLDS NUMBERS

Ezgi Orbay Akcengiz[1]
METUWIND
Ankara, Turkey

Ezgi Aslan[2]
METU
Ankara, Turkey

Nilay Sezer Uzol[3]
METU
Ankara, Turkey

ABSTRACT

In this study, Computational Fluid Dynamics simulations of flow around thick have been performed. Thick airfoils are generally preferred in wind turbine blades for structural and aerodynamic performances. High Reynolds flows around thick airfoils are one of the challenging problems in wind turbine blade design due to turbulent, separated and complex flow field characteristics. In the CFD analyses, both 2-D RANS simulation approach on structured computational grids is considered. Grid sensitivity study is also performed and presented in this paper.

INTRODUCTION

Thick airfoils are generally preferred in the blade design of large wind turbines. The thickness of the airfoil increases in the outer parts of the blade in terms of aerodynamic performance and near the root section of the blades in terms of both structural and aerodynamic performance requirements. The aerodynamic design of wind turbine rotors are generally fast Blade Element Momentum Theory (BEM) analysis. In this analysis, obtaining accurate lift and drag polars for a wide range of Reynolds numbers and all angles of attacks from -180^o to 180^o are necessary. For a typical modern non-linearly twisted and tapered blade, usually there is a distribution of a family of airfoils along the radius. Airfoil aerodynamic characteristics are generally obtained through a combination of numerical simulations and wind tunnel tests during both airfoil design and blade design processes. Because of the limited availability of wind tunnel data in limited Reynolds number ranges, obtaining accurate numerical results is of vital importance. Accurate aerodynamic characteristics for this type of airfoils are challenging to be obtained both by experiments and numerical analyses due to highly separated flows. The flow around wind turbine blades are characterized by low Mach number and high Reynolds numbers (Re). Reynolds number varies from 1 to 15 Million depending on the chord length of the blade profile. Investigating turbulent and complex flow field in high Reynolds number flows by experiments are difficult to obtain and more expensive. Therefore, obtaining the accurate lift and drag polars of airfoils in high Reynolds numbers and a wide range of angles of attacks plays an important

[1] Instructor in METUWIND, PhD candidate in Department of Aerospace Engineering, METU, Email: eorbay@metu.edu.tr
[2] PhD student in Department of Aerospace Engineering, METU, Email: ezgi.aslan@metu.edu.tr
[3] Assoc. Prof. Dr. in Department of Aerospace Engineering, METU, Email: nuzol@metu.edu.tr

role in the wind turbine blade design. In the literature, the number of researchers focusing on numerical simulation of high Reynolds flows around thick airfoil has been increasing. The summary of studies focused on thick airfoils in the literature is can be found in Table 1. Baldaccchino [Baldacchino et al., 2016] investigated aerodynamic performance of two different airfoils by solving incompressible RANS equations in different CFD solvers. SST turbulence model was used with transition models and as fully turbulent flow. Lehmkuhl [Lehmkuhl et al., 2014] investigated pre-stall and post-stall behavior of different thick wind turbine airfoils at $Re=3x10^6$ by using LES. In another study [Volikas et al., 2019], a comparison of different turbulence models used in the RANS simulations were conducted for the S809 airfoil at $Re = 2x10^6$. Comparison of RANS and DES simulations for a very thick airfoil, DU00-W-401, at high Reynolds numbers was done by Bangga [Bangga et al., 2018]. They concluded that 3-D DES simulations provided better agreement than 2D RANS simulations. In 2009, the flow field around DU 97-W-300 was investigated by solving unsteady RANS equations [Barone et al., 2009]. The same airfoil was used with different airfoils by unsteady RANS simulations in 2012 [Xu et al., 2014]. Colonia [Colonia et al., 2016] studied on the calibration of transition model to improve the prediction of transition on DU00-W-212 airfoil for 2-D steady RANS simulations. FFA-W3-241 is investigated by different researchers [Campobasso et al., 2008, Sorenson et al., 2014, Prospathopoulus et al., 2014]. Campobasso and Sorenson preferred to use steady state RANS method, Prospathopoulus solved both steady-state and unsteady RANS equations. In 2016, [Sorenson et al, 2016] presented the simulations results for the EU AVATAR project, in order to establish the necessary requirements to obtain consistent lift over drag ratios among seven CFD codes. The flow around a 2-D airfoil case of DU00-W-212 was studied, for both transitional and fully turbulent conditions at Reynolds numbers of 3×10^6 and 15×10^6. Compressible and incompressible Reynolds Averaged Navier-Stokes equations solved and SST turbulence model with different types of transition models are used. They discussed the necessary grid resolution as a result of grid refinement study, domain size by using different proximity of far field boundary and iterative convergence criteria to have consistent results, and suggestions were given for best practice.

Table 1. A brief summary of literature on numerical analysis of thick airfoil

Author	**Airfoil**	**Re ($x10^6$)**
Baldacchino, 2016	DU97-W-300	2
Bangga, 2018	DU00-W2-401	3
Bangga, 2018	DU91-W2-250, DU97-W-300, DU00-W2-350, DU00-W2-401	3, 17.6
Barone, 2009	DU97-W-300	3
Campobasso, 2008	FFA-W3-241	1.6
Colonia, 2017	DU00-w-212	3, 9, 15
Lehmkuhl, 2014	DU-93-W-210, DU-91-W2-250 and FX-77-W-500	3
Prospathopoulos, 2014	FFA-W3-241, FFA-W3-301, FFA-360, NACA 63-018	3, 6, 8, 10, 12, 15, 20
Rogowski, 2018	DU91-W2-250	3
Sorenson, 2014	FFA-W3-301 and FFA-W3-360	3
Sorenson, 2016	DU00-W-212	3, 15
Xu, 2014	DU-91-W2-250, DU-97-W-300, DU-96-W-350	3
Zahle, 2014	LRP2-30, LRP2-36	3, 6, 9

In this study, flow field characteristics around a thick airfoil, DU00-W-212, is investigated by performing CFD simulations with RANS. The geometry of airfoil can be seen from Figure 1. In the simulations, 3 different test cases stated in AVATAR Blind Test Campaign (Table 2), Re=3x10^6, 6x10^6, 9x10^6, and angles of attacks from 0^o to 20^o are considered. CFD analysis are performed by using a commercial CFD solver, CFD++ and an open-source CFD solver, SU2. The results are compared with experimental data available in the literature and XFOIL calculations.

In Computational Fluid Dynamics analysis, the generation of the computational grid has a very important place. During the analysis, discretization errors are mainly caused by two factors: discretization of solution domain and discretization of equations solved. Discretization in space for Finite Volume Methods means the subdivision procedure of the domain into small control volumes [Jasak, 1994]. In order to reduce the errors caused by grid properties, the CFD analysis results should be independent of computational grid. A systematic grid sensitivity analysis should be performed for accurate simulations. Therefore, grid independence study is also performed by using CFD++.

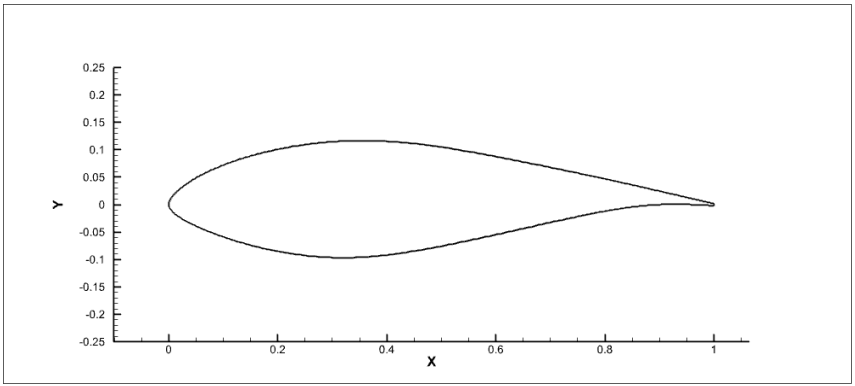

Figure 1: Geometry of DU00-W-212

Table 2. Test cases in AVATAR Blind Test Campaign [Ceyhan, O. & Pires, O. 2015]

Test No	Re	Mach
1	3 M	0.075
2	6 M	0.054
3	6 M	0.029
4	9 M	0.082
5	9 M	0.044
6	12 M	0.058
7	15 M	0.080

METHODOLGY

Grid Generation

2-D computational grids with quadrilateral cells around airfoil is generated in Pointwise. O-type grid topology is applied in order to ensure orthogonality of grid cells. Structured grid cells are extruded from airfoil surfaces to outer boundary.

Grid sensitivity analysis is performed by generating 9 different grids from very coarse to very fine. Grid cell size is increased and decreased by a factor of √2, so the area of a cell is doubled or halved. The change in the cell edge size is performed in every direction by keeping growth ratio (1.08) and domain size (40 chords) as constant. Detailed information about generated computational grids are given in Table 3. Zoomed view of grids around airfoil can be seen in Figure 2. In Figure 3 and 4, Grid structures for Grid 3 and Grid 9 are given with detailed views of Trailing Edge (TE) and Leading Edge (LE).

Effect of far field boundary position is also investigated. By keeping grid structure same (Grid 3 :768 x 202) with same initial cell size ($7.50x10^{-7}$), location of far field is changed from 5 chords to 60 chords. The effect is evaluated in terms of lift (C_l) and drag coefficient (C_d) comparison between different locations of far filed boundary.

CFD Analysis Details

The CFD simulations have been performed by using a commercial CFD solver, CFD++ and an open source CFD code, SU2. In both CFD solvers, 2-D RANS equations are solved with k-ω SST turbulence model for fully turbulent flow. Adiabatic Viscous Wall BC is applied on airfoil surface and characteristic-based Inflow/Outflow BC is given for far field.

Grid sensitivity analysis is performed in CFD++. Since the simulations are run at very small values of Mach number (M<0.1), Preconditioned Pressure-based Compressible Navier-Stokes solver is applied. Point-Implicit method is used for steady-state simulations. Multi-grid acceleration scheme of W-Cycle type is used with 9 levels. Steady state simulations in CFD++ have been conducted until residual RMS Error values reduce to 10^{-5}. Turbulence level is $8.16x10^{-4}$ as in the literature. Advanced Two-layer wall function is applied on the airfoil surface.

The ROE method is used in SU2. Since it is a wind turbine airfoil, we have subsonic flow regime with a maximum Mach number of 0.082 and ROE gives good enough results when compared with the experimental data. The maximum number of iterations are limited up to 1000. The convergence is achieved after around 400 iterations and simulations are continued up to maximum iteration number. No CFL adaptation is used and the most suitable CFL is chosen manually as 200 by trial and error. For the linear solver, FMGRES option is chosen in SU2 which is actually the Gauss-Siedel method. The inner iteration of linear solver is set as 10. W-Cycle Multigrid with 9 levels are used. MUSCL flow option is applied for the flow, but not for the turbulence. Euler implicit method is used for the time discretization. For the turbulence, scalar upwind is applied.

In addition to CFD solvers, panel method calculations by XFOIL for lift and drag polars are performed. The critical N value in e^N method value is taken as 9. This value means an average wind tunnel testing and laminar flow. The iteration number is 200 in XFOIL. Reynolds number, Mach number and Angle of attacks are chosen as in the CFD solvers.

Table 3. Detailed information about computational grids generated for Grid Sensitivity Analysis

Grid. No (O-type)	Domain Size (chord)	Number of Grid Cells on airfoil	Number of Grid Cells normal to the wall	First Cell Size in the normal direction	Strecthing Ratio	Total Number of Grid Cells	Y+	Time consumption for 1 iteration step at Case 1 (sec)
Grid 1	40	1536	211	3.75E-07	1.08	322560	0.023	5.0
Grid 2	40	1086	205	5.30E-07	1.08	222630	0.029	3.3
Grid 3	**40**	**768**	**202**	**7.50E-07**	**1.08**	**154368**	**0.037**	**2.1**
Grid 4	40	543	197	1.06E-06	1.08	106232	0.051	1.6
Grid 5	40	384	192	1.50E-06	1.08	73153	0.084	1.2
Grid 6	40	271	188	2.12E-06	1.08	50677	0.119	0.9
Grid 7	40	192	184	3.00E-06	1.08	35136	0.169	0.7
Grid 8	40	136	180	4.24E-06	1.08	23986	0.241	0.5
Grid 9	40	96	175	6.00E-06	1.08	16356	0.342	0.3

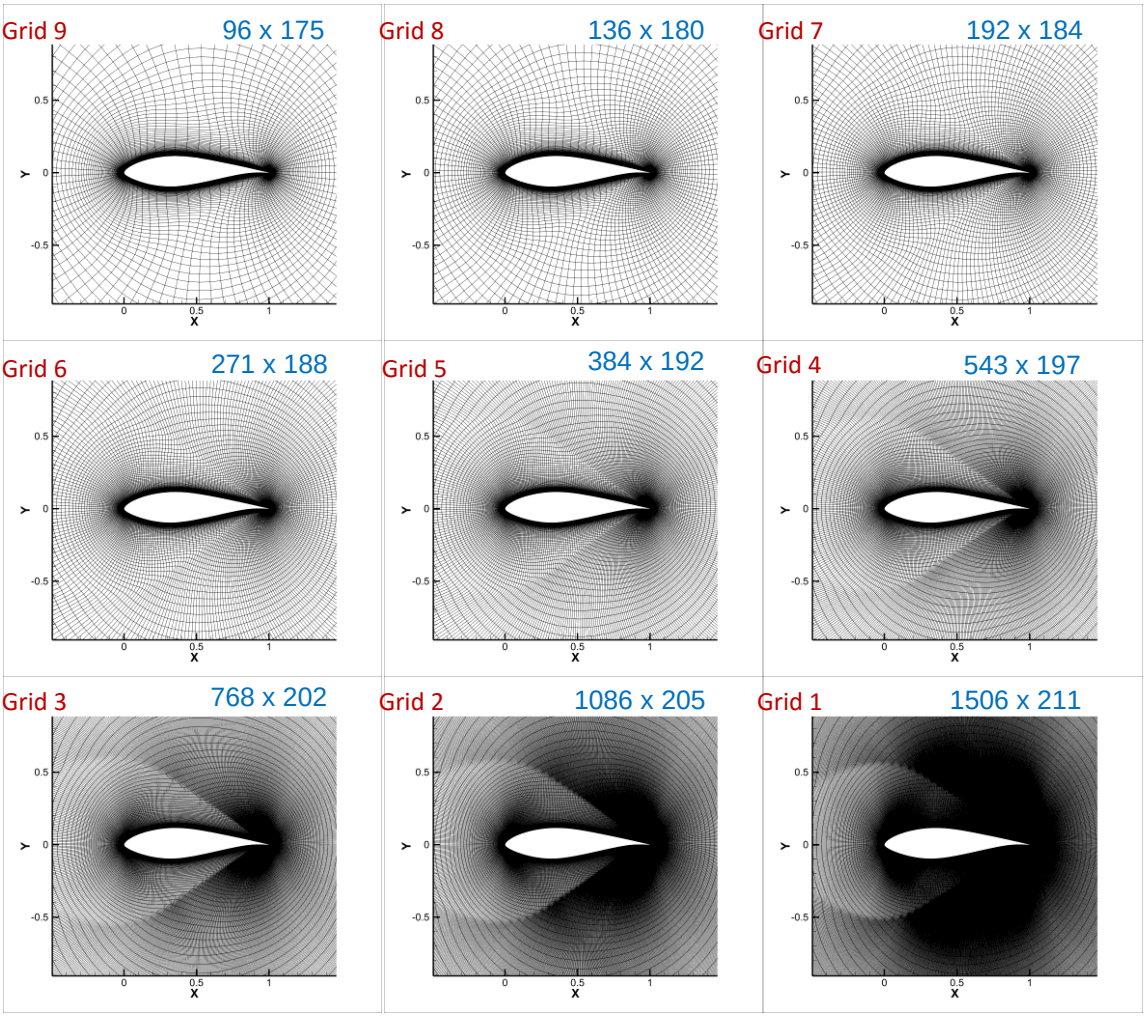

Figure 2: Computational grids around airfoil

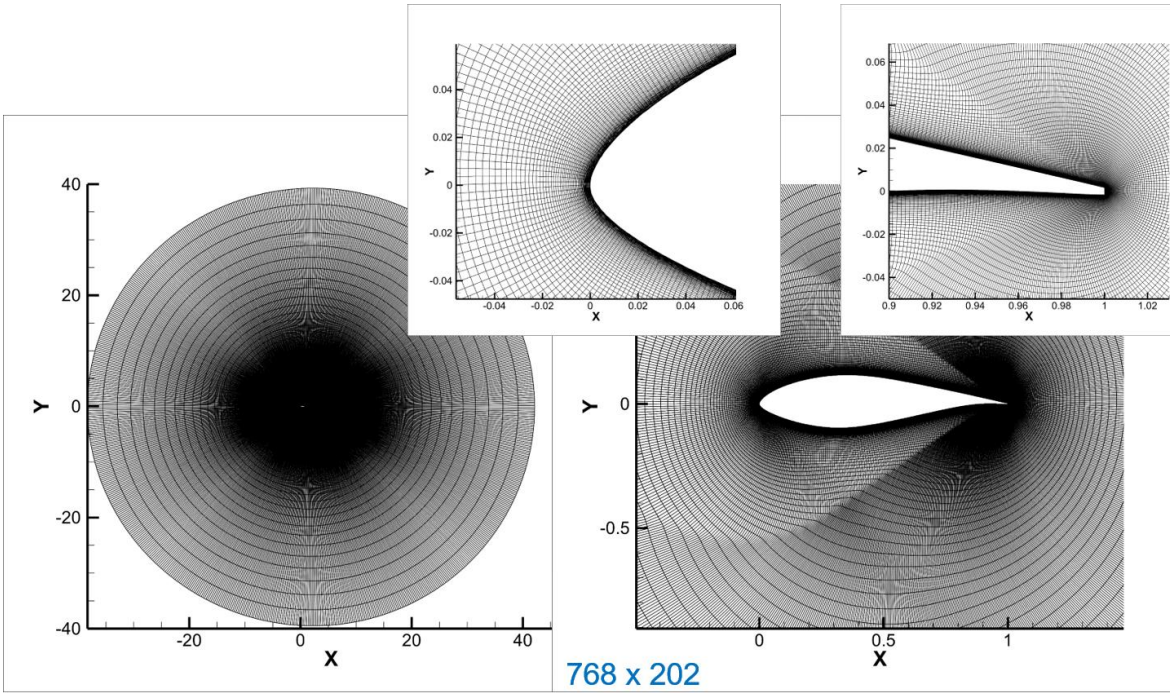

Figure 3: Grid structures around TE and LE of Grid 3

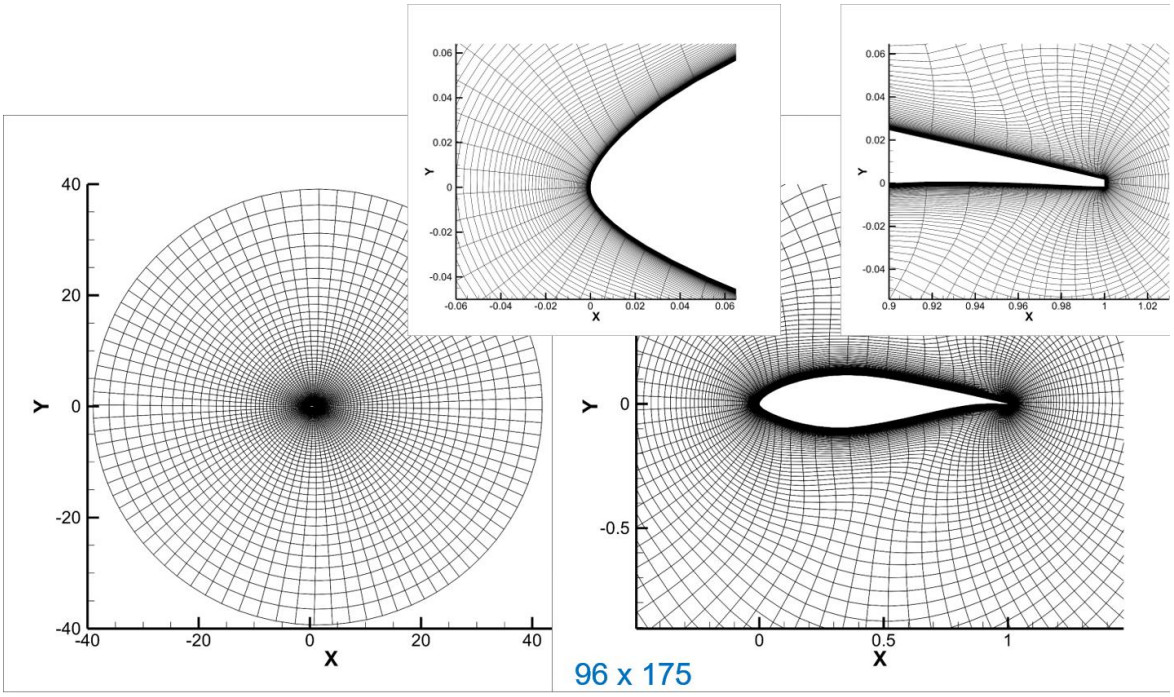

Figure 4: Grid structures around TE and LE of Grid 9

RESULTS

Grid Sensitivity Analysis

In this section, the results of grid sensitivity study obtained by CFD++ are presented. In Figure 5, Residual plot for grid independence study is given while in Figure 6, Typical convergence plots for grid independence study are given for lift coefficient and drag coefficient. Grid sensitivity analysis for 2-D RANS simulation by CFD++ can be seen in terms of C_l and C_d variations with respect to angle of attack at Re = 3M can be seen from Figure 7 and 8, respectively. Similarly, Figure 9 and 10 show results obtained for 2-D RANS simulation by CFD++ can be seen in terms of C_l and C_d variations with respect to angle of attack at Re = 6M, and Figure 11 and 12 present results obtained for 2-D RANS simulation by CFD++ can be seen in terms of C_l and C_d variations with respect to angle of attack at Re = 9M. At linear region, values are very close to each other. As angle of attack increases, difference also increases, especially at stall region. From the plots, from grid 9, 8, 7, 6, 5 are visible. Despite of the fact that difference between C_l and C_d values of computational grids increases with Reynolds numbers, similar convergence behavior can be observed for Re = 3M, 6M and 9M. Grid 3 is seen as most converged grid, especially for highest Reynolds number. Therefore, it is chosen for further simulations.

In Figure 13, effects of Reynolds numbers on aerodynamic performance of airfoil is presented. Numerical analysis results obtained for Grid 3 are compared with experimental measurements available in the literature. Numerical results are over-predicting the experiments at stall region as also known in the literature, with such steady RANS k-omega simulations. However, it can be seen that the Reynolds number dependency trends predicted reasonably well. Since, Reynolds number gives the ratio of inertia forces to viscous forces, as Reynolds number increases, the effect of viscous forces decreases and flow separation is delayed to higher angle of attacks. Therefore, it can be seen from Figure 13 that as Reynolds number increases, maximum C_l (C_{lmax}) and stall angle increases.

Flow field around DU00-W-212 can be observed in terms of shear stress distribution, vorticity magnitude and C_p distribution contours at two different high angles of attack (16^o and 20^o) for Re = 3M, 6M and 9M in Figure 14, 15 and 16, respectively. Separation occurs at the point where shear stress on the surface is 0, which means the change of x-component of velocity vector in y-axis is 0. Flow is separated from surface and separation region or recirculation region are formed. In the related figures, the separation points and reattachment points are indicated. As angle of attacks increases, separation point is getting closer to LE. In the analysis, it is observed that there are very small differences in the location of separation point as Reynolds number changes from $3x10^6$ to $9x10^6$. Separated flow can be also observed in these figures. In Figure 17, 18 and 19, C_p distribution over airfoil surfaces at Re = 3M, 6M and 9M are given. The separation can be observed at the point where C_p does not change with location in x-axis. In the graphics, separation point is shifted from 0.35 chords to 0.45 chords as Reynolds number changes from $3x10^6$ to $9x10^6$. Numerical results are also compared with experimental data in terms of C_p distribution.

In Figure 20, the effect of proximity of far field boundary is presented in terms of C_l and C_d comparison for 4 different angles of attacks; 0^o,7^o, 14^o and 18^o. Difference in C_l decreases as far field boundary is located at least 20 chords from airfoil. However, Difference in C_d is much higher, convergence is obtained after 40 chords. Therefore, it can be said that far field boundary can be located at least 40 chords away from airfoil surface for such O-type grids.

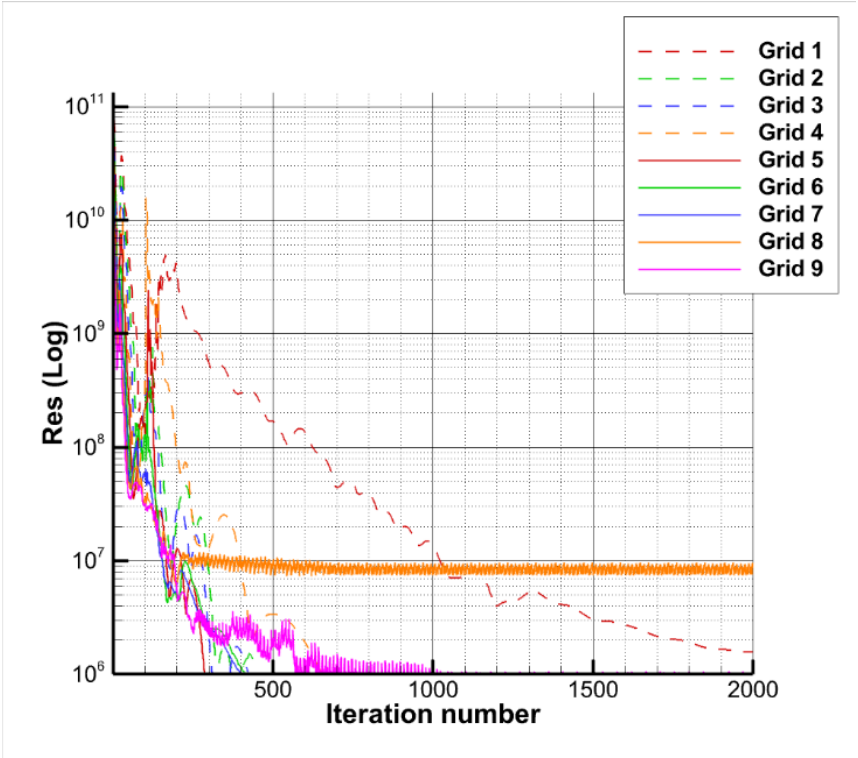

Figure 5: Residual graph for grid independence study (CFD++)

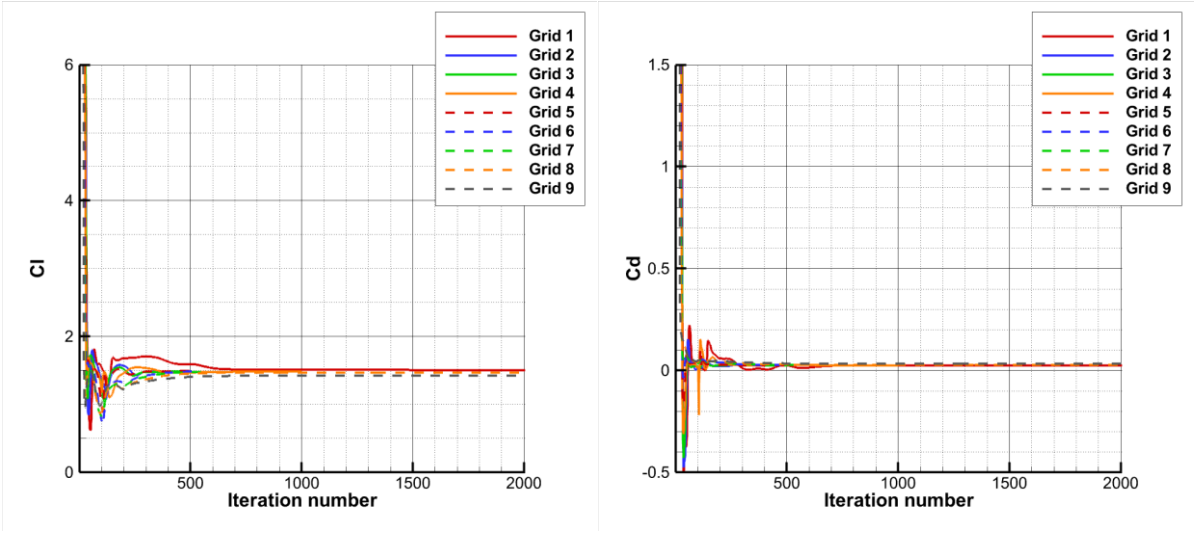

Figure 6: Typical C_l and C_d convergence history for grid independence study (CFD++)

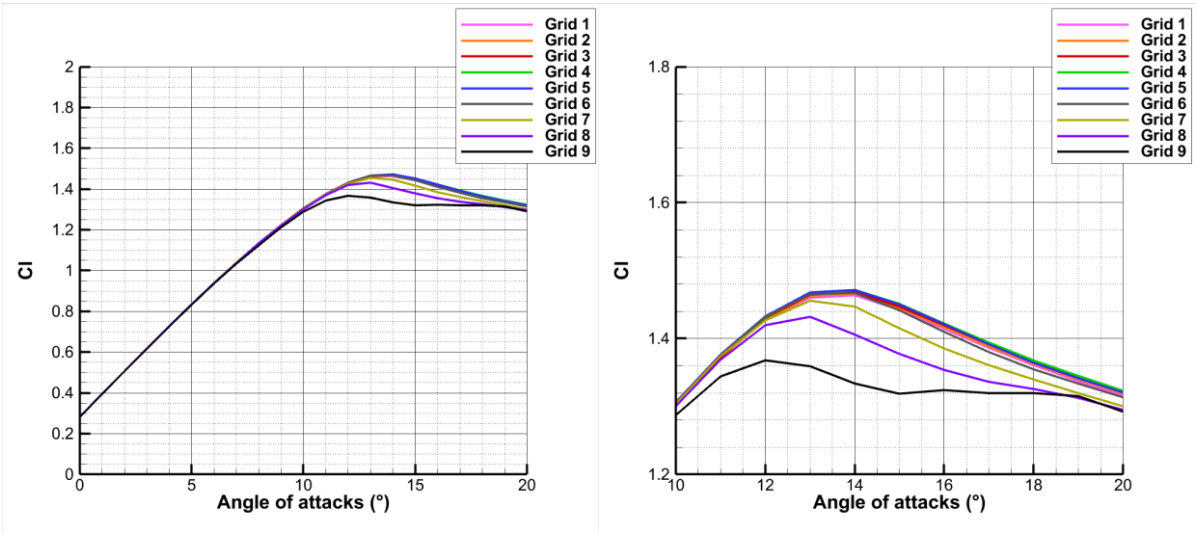

Figure 7: C_l comparison for grid independence study at Re=3M performed by CFD++ (RHS: a zoomed view for stall region)

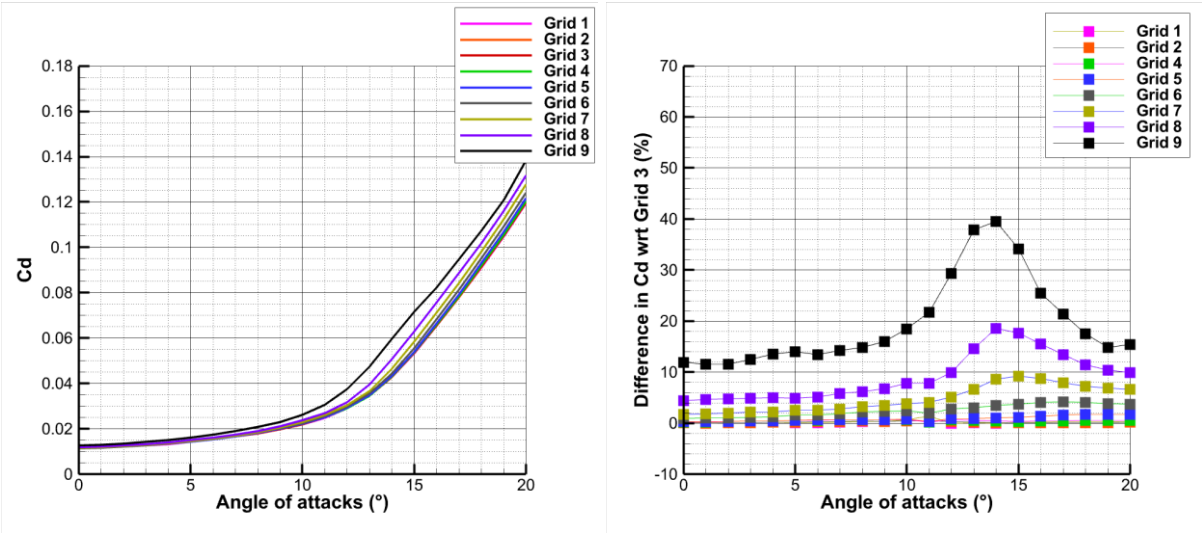

Figure 8: C_d comparison for grid independence study at Re=3M performed by CFD++ (RHS: C_d Difference between grids with respect to Grid 3)

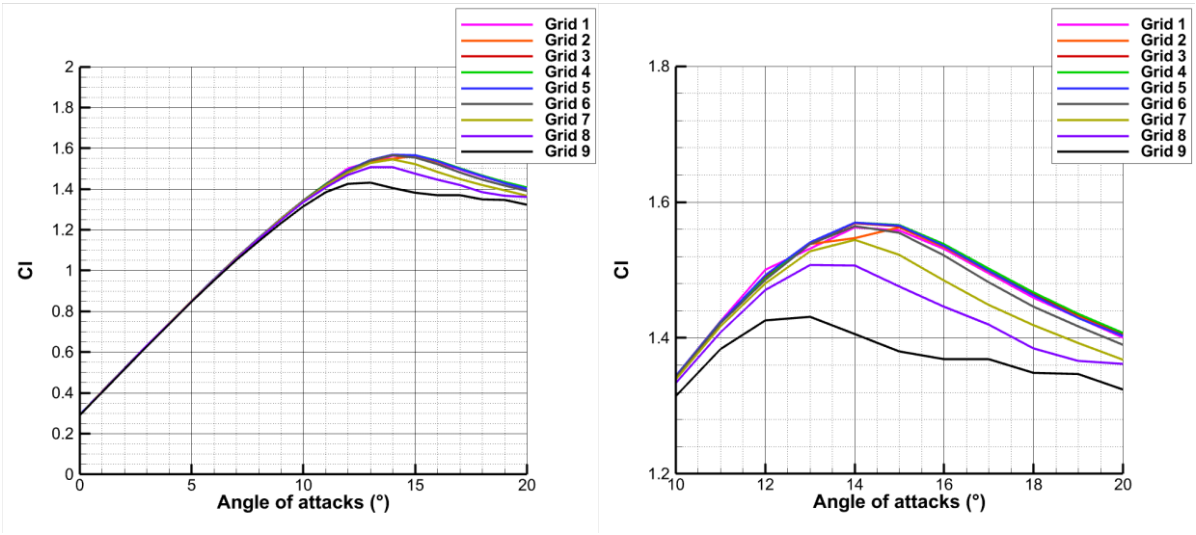

Figure 9: C_l comparison for grid independence study at Re=6M performed by CFD++ (RHS: a zoomed view for stall region)

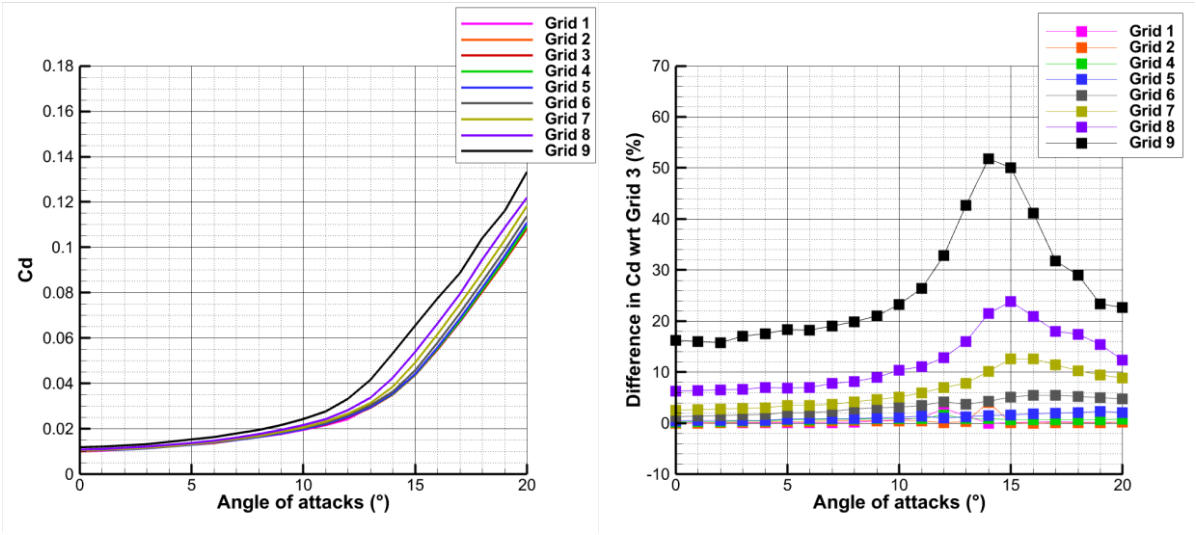

Figure 10: C_d comparison for grid independence study at Re=6M performed by CFD++ (RHS: C_d Difference between grids with respect to Grid 3)

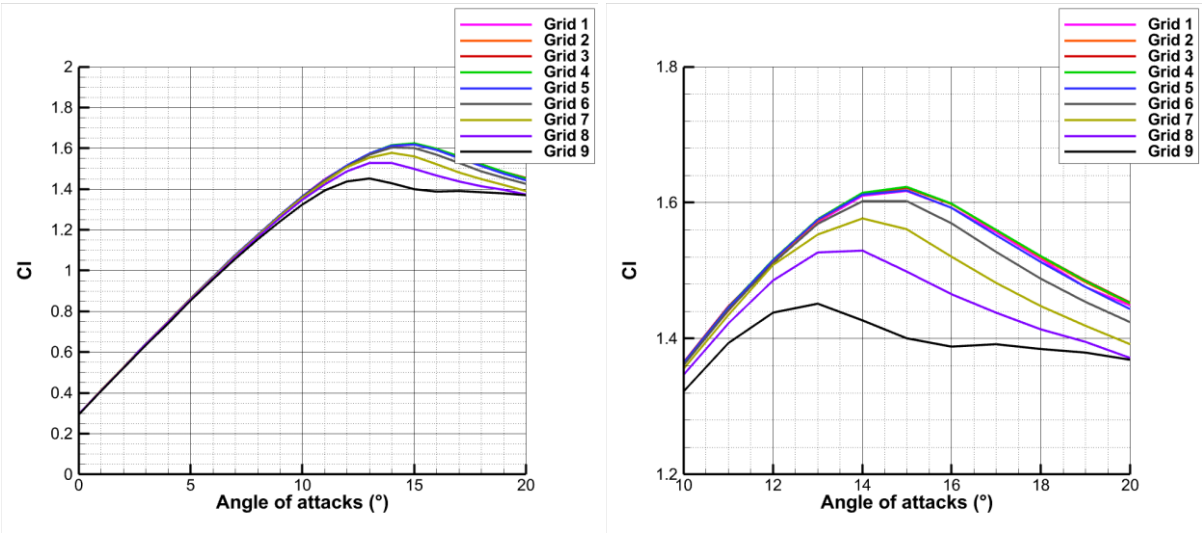

Figure 11: C_l comparison for grid independence study at Re=9M performed by CFD++ (RHS: a zoomed view for stall region)

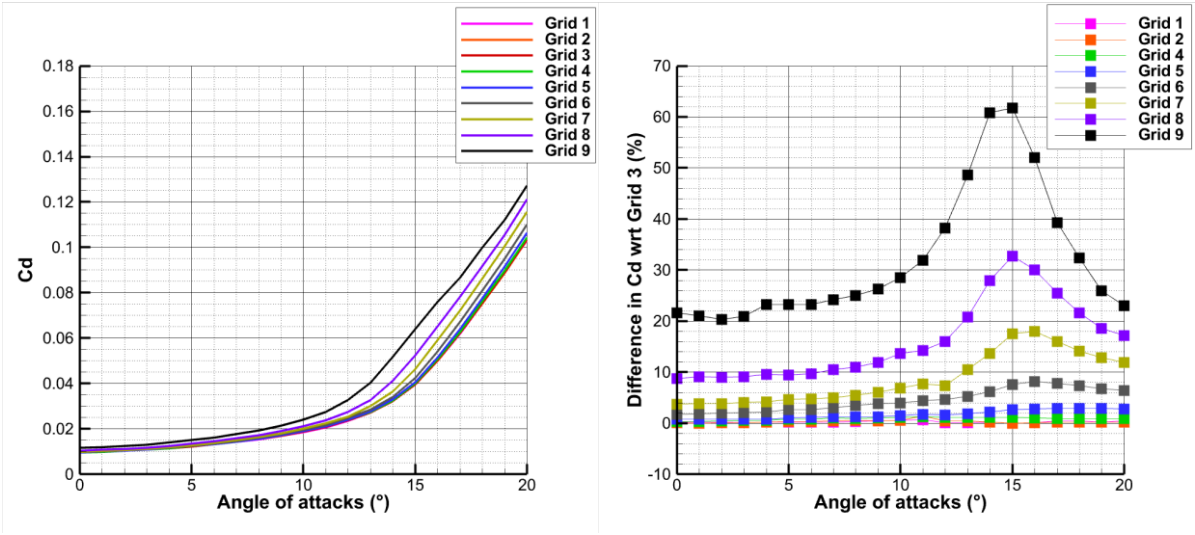

Figure 12: C_d comparison for grid independence study at Re=9M performed by CFD++ (RHS: C_d Difference between grids with respect to Grid 3)

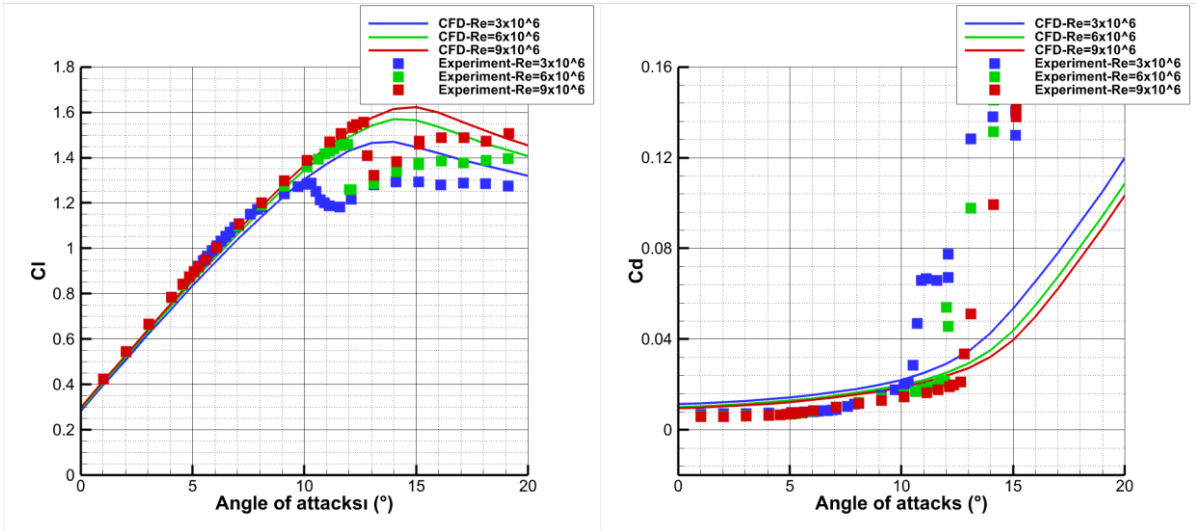

Figure 13: Effect of reynolds number (for Grid 3 by CFD++)

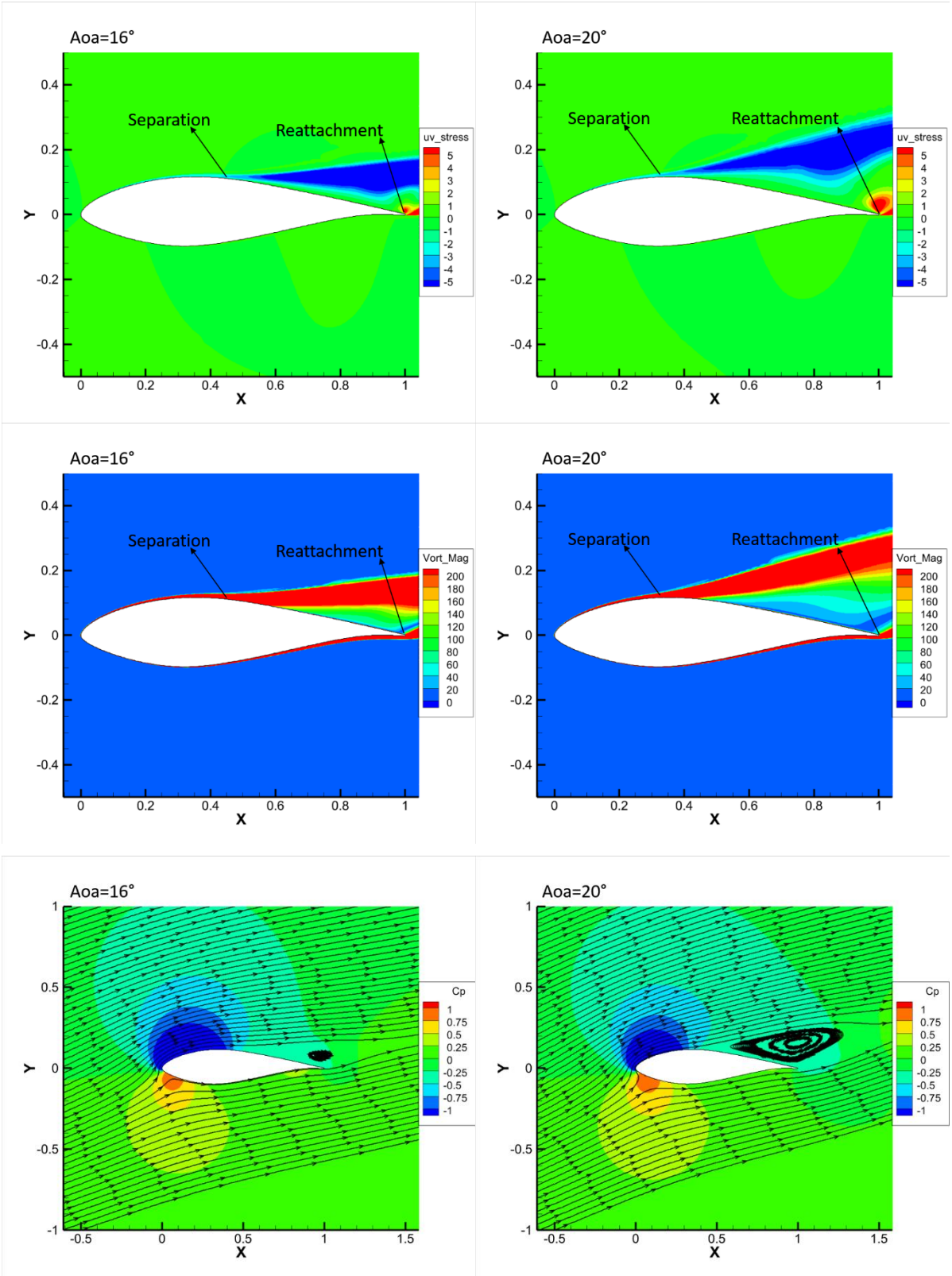

Figure 14: Shear stress distribution, Vorticity magnitude and Pressure coefficient contours for Grid 3 at different AoAs and Re = 3M (CFD++)

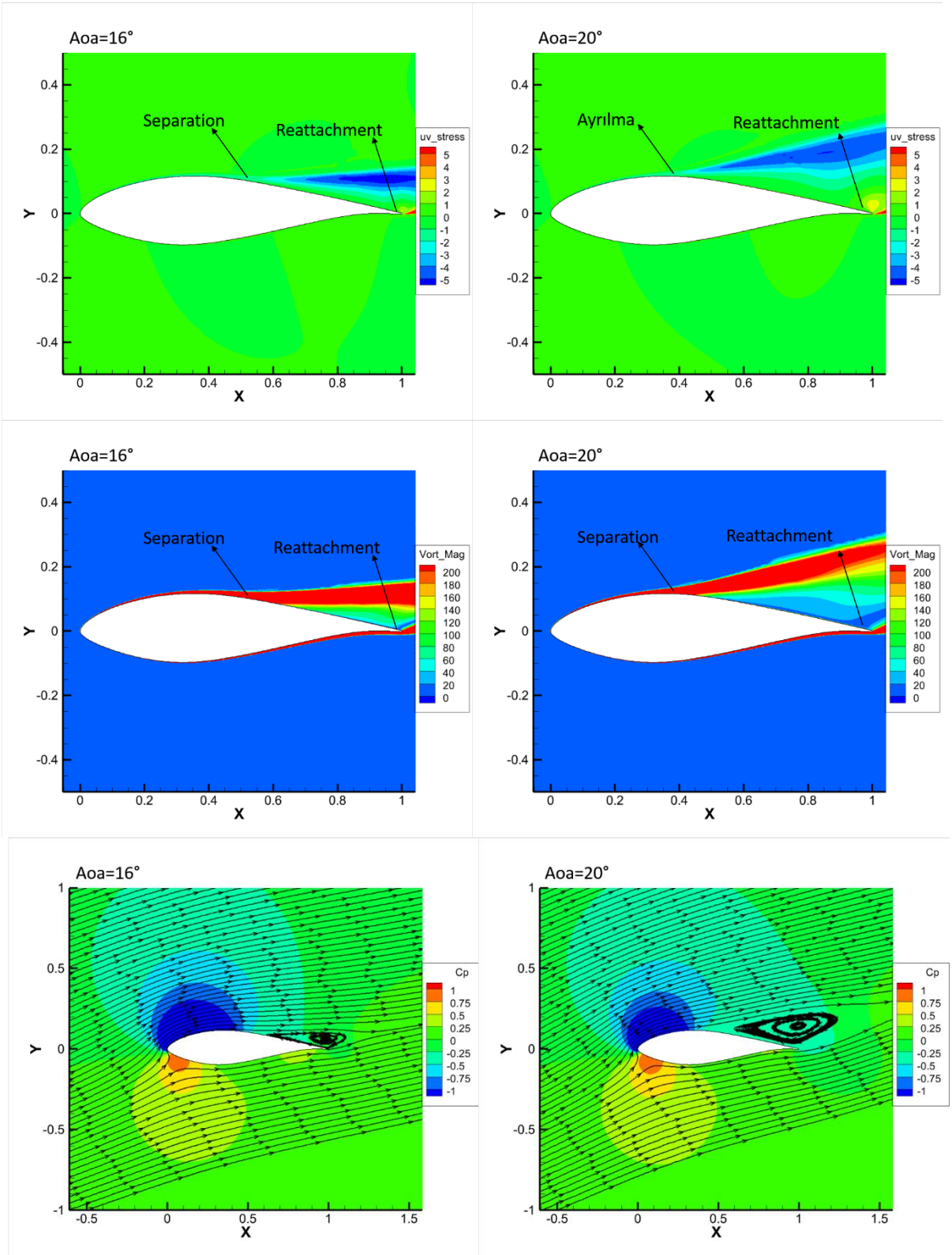

Figure 15: Shear stress distribution, Vorticity magnitude and Pressure coefficient contours for Grid 3 at different AoAs and Re = 6M (CFD++)

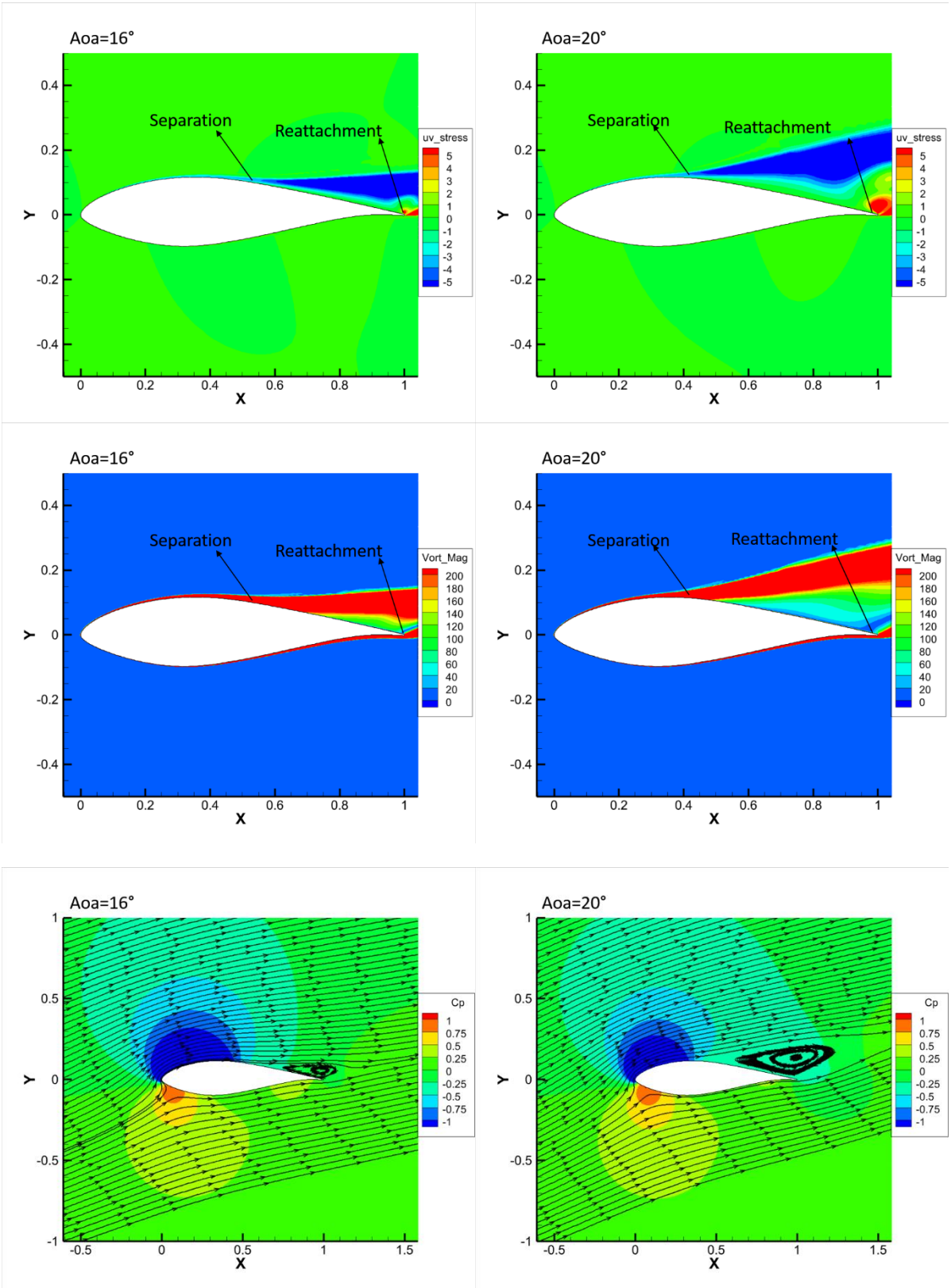

Figure 16: Shear stress distribution, Vorticity magnitude and Pressure coefficient contours for Grid 3 at different AoAs and Re = 9M (CFD++)

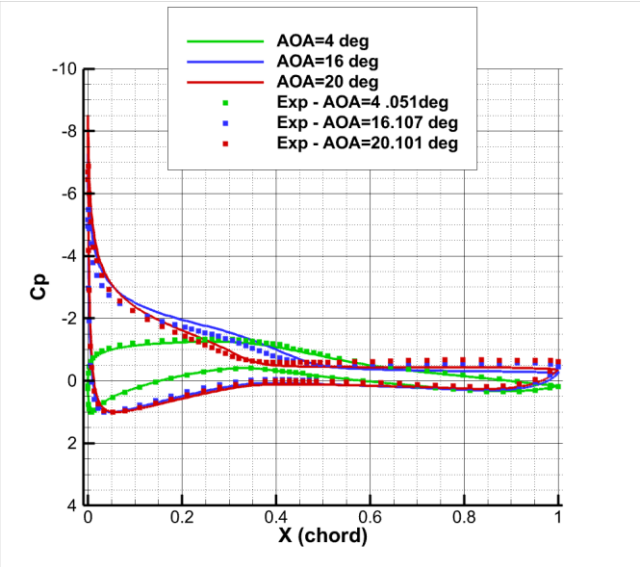

Figure 17: Cp distribution over airfoil surfaces at Re = 3M (CFD++)

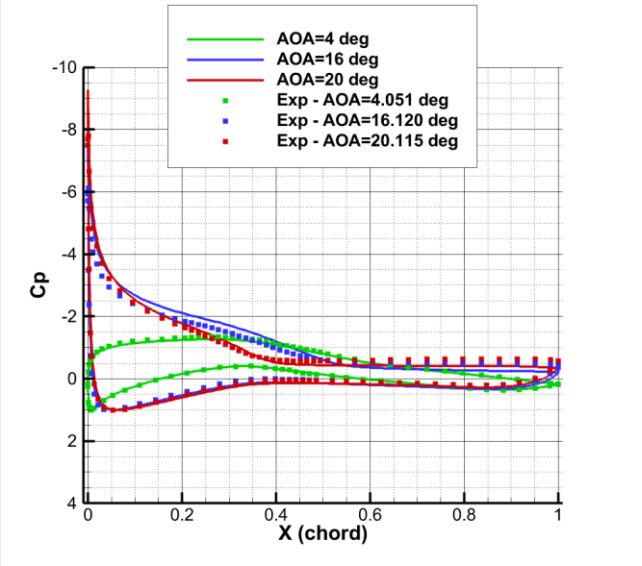

Figure 18: Cp distribution over airfoil surfaces at Re = 6M (CFD++)

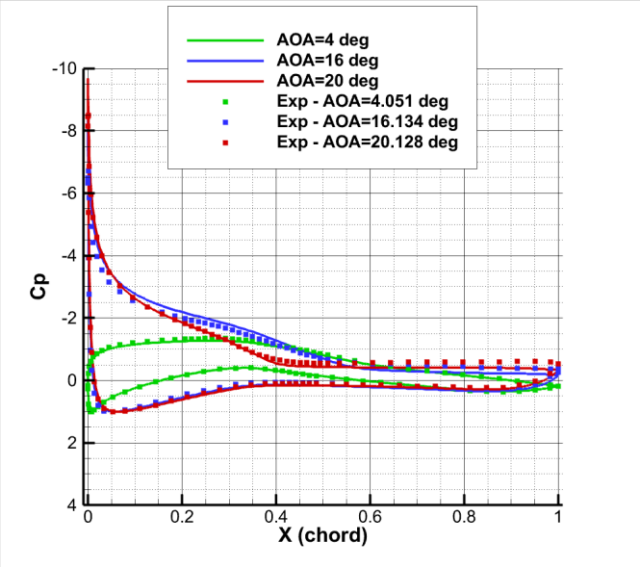

Figure 19: Cp distribution over airfoil surfaces at Re = 9M (CFD++)

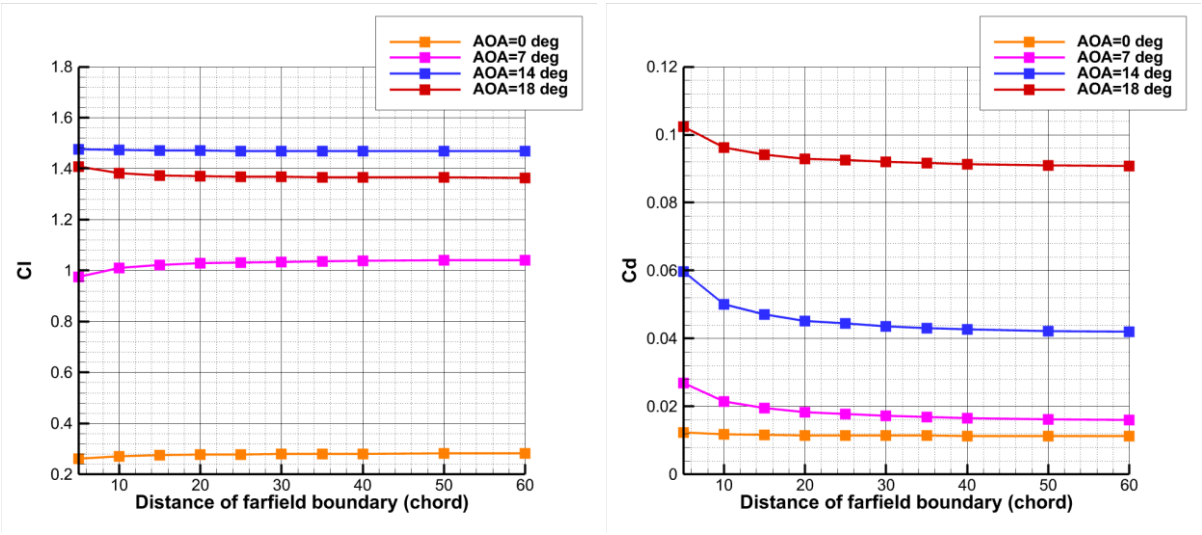

Figure 20: Effect of proximity of farfield boundary (CFD++)

Comparison of CFD++ results with SU2 and XFOIL

In this subsection, the comparison of results obtained by SU2, CFD++, XFOIL and experimental data is presented. Figures 21, 22 and 23 show C_l and C_d comparison at Re = 3M, 6M and 9M, respectively. Both CFD solvers and XFOIL are weak to obtain accurate results at pre-stall and post-stall region with 2-D steady-state RANS simulations. At linear region, CFD++ gives more reasonable results compared to SU2 and XFOIL.

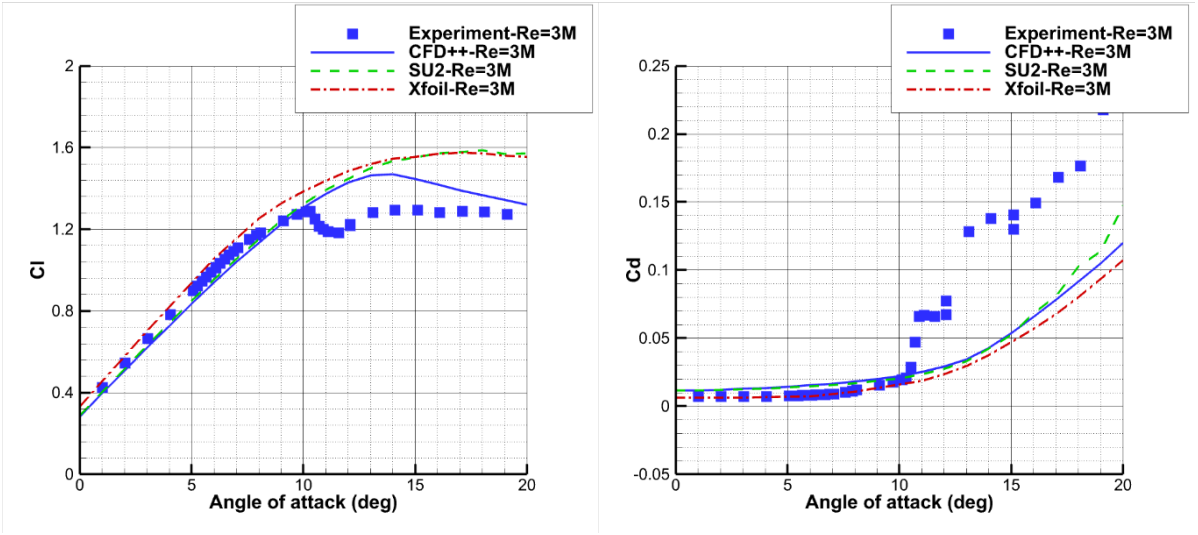

Figure 21: Comparison of CFD++, SU2, XFOIL and experimental data (Re = 3M)

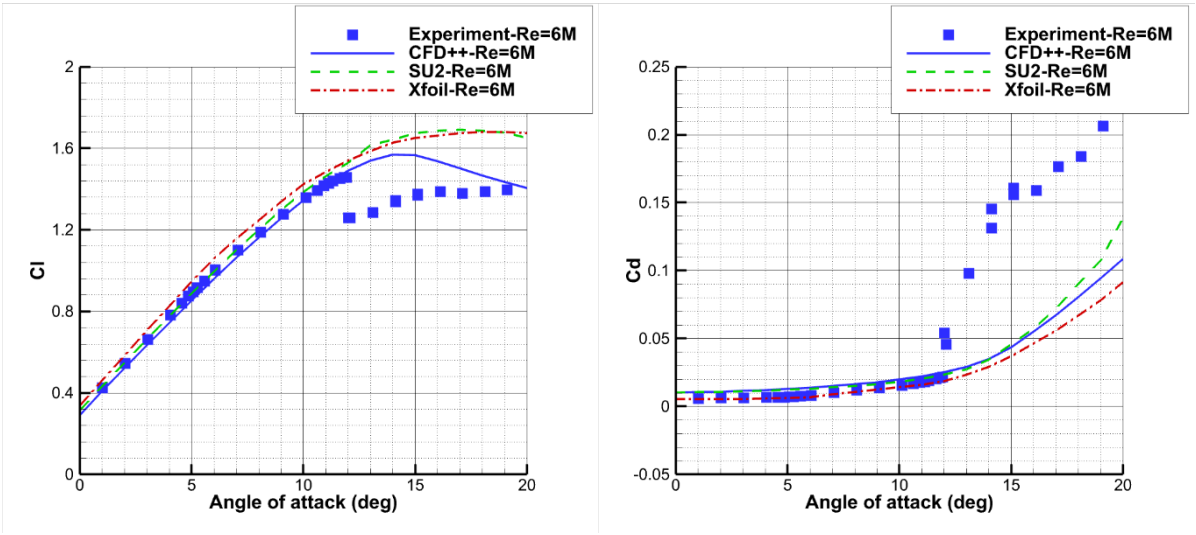

Figure 22: Comparison of CFD++, SU2, XFOIL and experimental data (Re = 6M)

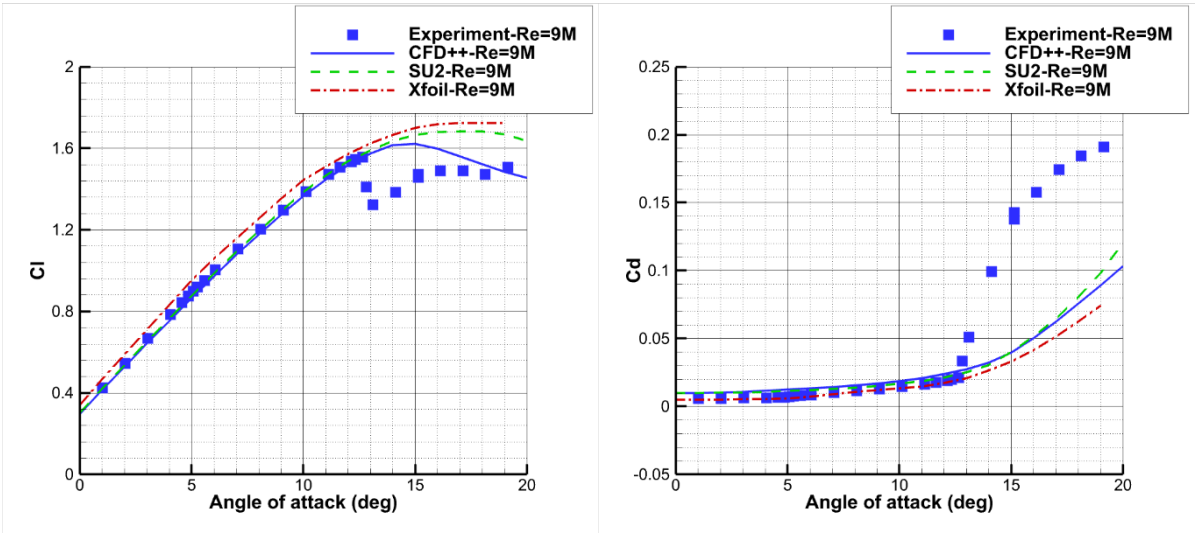

Figure 23: Comparison of CFD++, SU2, XFOIL and experimental data (Re = 9M)

CONCLUSION

Turbulent flow and separated flow conditions at high angle of attack and stall conditions are challenging for steady-state CFD simulations with RANS. For accurate numerical analysis, proper grid study should be performed for each Re numbers and airfoils. In this study, CFD grid independence study with structured O-grids is performed for DU 00-W-212 airfoil for 3 different Reynolds numbers of 3 M, 6 M & 9 M from moderate to high. The numerical results are obtained by both a commercial software and an open source CFD solver. Also results are compared with XFOIL and experimental data obtained from literature. As future work, in order to increase accuracy of predictions, transition models can be transition models can be added to 2D RANS analysis. Also, 3D simulations can be performed with DES or LES. A special refinement process can be done for wake region.

References

Baldacchino, D., Manolesos, M., Ferreira, C., Salcedo, A. G., Aparicio, M., Chaviaropoulos, T., ... & van Zuijlen, A. 2016. *Experimental benchmark and code validation for airfoils equipped with passive vortex generators*. In Journal of Physics: Conference Series (Vol. 753, No. 2, p. 022002). IOP Publishing.

Bangga, G., Lutz, T., & Krämer, E. 2018. *Active separation control on a very thick wind turbine airfoil-A URANS and DDES perspective*. In Journal of Physics: Conference Series (Vol. 1037, No. 2, p. 022025). IOP Publishing.

Bangga, G., Kusumadewi, T., Hutomo, G., Sabila, A., Syawitri, T., Setiadi, H., ... & Kristiadi, S. 2018. *Improving a two-equation eddy-viscosity turbulence model to predict the aerodynamic performance of thick wind turbine airfoils*. In Journal of Physics: Conference Series (Vol. 974, No. 1, p. 012019). IOP Publishing.

Barone, M., & Berg, D. 2009. *Aerodynamic and aeroacoustic properties of a flatback airfoil: an update*. In 47th AIAA Aerospace Sciences Meeting including The New Horizons Forum and Aerospace Exposition (p. 271).

Bartl, J., Sagmo, K. F., Bracchi, T., & Sætran, L. 2019. *Performance of the NREL S826 airfoil at low to moderate Reynolds numbers—A reference experiment for CFD models.* European Journal of Mechanics-B/Fluids, 75, 180-192.

Campobasso, M. S., Zanon, A., Foerster, M., Fraysse, F., & Bonfiglioli, A. 2008. *CFD modelling of wind turbine airfoil aerodynamics*. In: 63th ATI National Congress, Energia per lo sviluppo sostenibile, Palermo, Italy, 23-26 September 2008.

Ceyhan, O., & Pires, O. 2015. *Avatar blind test campaign*. EWEA 2015.

CFD++ Software, http://www.metacomptech.com/index.php/features/icfd

Colonia, S., Leble, V., Steijl, R., & Barakos, G. 2016. *Calibration of the 7—Equation Transition Model for High Reynolds Flows at Low Mach*. In Journal of Physics: Conference Series (Vol. 753, No. 8, p. 082027). IOP Publishing.

Geng, F., Kalkman, I., Suiker, A. S. J., & Blocken, B. 2018. *Sensitivity analysis of airfoil aerodynamics during pitching motion at a Reynolds number of 1.35× 105*. Journal of Wind Engineering and Industrial Aerodynamics, 183, 315-332.

Jasak, H. 1996. *Error analysis and estimation for the finite volume method with applications to fluid flows*. PhD Thesis, Imperial College London (University of London).

Lehmkuhl, O., Calafell, J., Rodríguez, I., & Oliva, A. 2014. *Large-Eddy Simulations of wind turbine dedicated airfoils at high Reynolds numbers*. In Wind Energy-Impact of Turbulence (pp. 147-152). Springer, Berlin, Heidelberg.

Pointwise Software, https://www.pointwise.com/

Prospathopoulos, J. M., Papadakis, G., Sieros, G., Voutsinas, S. G., Chaviaropoulos, T. K., & Diakakis, K. 2014. *Assessment of the aerodynamic characteristics of thick airfoils in high Reynolds and moderate Ma numbers using CFD modeling*. In Journal of Physics: Conference Series (Vol. 524, No. 1, p. 012015). IOP Publishing.

Rogowski, K., Hansen, M. O. L., Hansen, R., Piechna, J., & Lichota, P. 2018. *Detached Eddy Simulation Model for the DU-91-W2-250 Airfoil*. In Journal of Physics: Conference Series (Vol. 1037, No. 2, p. 022019). IOP Publishing.

Sørensen, N. N., Zahle, F., Bak, C., & Vronsky, T. 2014. *Prediction of the effect of vortex generators on airfoil performance*. In Journal of physics: conference series (Vol. 524, No. 1, p. 012019). IOP Publishing.

Sørensen, N. N., Mendez, B., Muñoz, A., Sieros, G., Jost, E., Lutz, T., ... & Ferreira, C. 2016. *CFD code comparison for 2D airfoil flows*. In Journal of Physics: Conference Series (Vol. 753, No. 8, p. 082019). IOP Publishing.

Volikas, A., Konstantinos-Stefanos, N. (2019), *Turbulence Modeling Investigation of Airfoil Designed for Wind Turbine Applications*, AIP Conference Proceedings 2123, 020067.

Xu, H., Shen, W., Zhu, W., Yang, H., & Liu, C. 2014. *Aerodynamic analysis of trailing edge enlarged wind turbine airfoils*. In Journal of Physics: Conference Series (Vol. 524, No. 1, p. 012010). IOP Publishing.

Zahle, F., Bak, C., Sørensen, N. N., Vronsky, T., & Gaudern, N. 2014. *Design of the LRP airfoil series using 2D CFD*. In Journal of Physics: Conference Series (Vol. 524, No. 1, p. 012020). IOP Publishing.